

Electronic Supplementary Material (ESI) for Journal of Materials Chemistry A.
This journal is © The Royal Society of Chemistry 2021

Electronic Supplementary Information:

Glycerol Oxidation Assisted Electrochemical CO₂ Reduction for the Dual Production of Formate

Yuhou Pei^{a,‡}, Zhenfeng Pi^{a,‡}, Heng Zhong^{*,a,b}, Jiong Cheng^a, Fangming Jin^{a,b,c}

^a School of Environmental Science and Engineering, State Key Lab of Metal Matrix Composites, Shanghai Jiao

Tong University, Shanghai 200240, P.R. China

^b Center of Hydrogen Science, Shanghai Jiao Tong University, Shanghai, 200240, P.R. China

^c Shanghai Institute of Pollution Control and Ecological Security, Shanghai 200092, P.R. China

**Corresponding author:*

Heng Zhong, Tel: +86-21-54745410, E-mail: zhong.h@sjtu.edu.cn

‡ These authors contributed equally to this work.

1. Additional Experimental Section

Chemicals and materials. Nickel (II) nitrate hexahydrate ($\text{Ni}(\text{NO}_3)_2 \cdot 6\text{H}_2\text{O}$, $\geq 98.0\%$, Macklin), cobalt (II) nitrate hexahydrate ($\text{Co}(\text{NO}_3)_2 \cdot 6\text{H}_2\text{O}$, $\geq 99.5\%$, Aladdin), urea ($(\text{NH}_2)_2\text{CO}$, 99.0% , Sinopharm), potassium hydroxide (KOH, $\geq 90.0\%$, Tansoole), glycerol ($\text{C}_3\text{H}_8\text{O}_3$, $\geq 99.5\%$, Macklin), formic acid (CH_2O_2 , 98% , Sinopharm), sodium sulfide ($\text{Na}_2\text{S} \cdot 9\text{H}_2\text{O}$, $\geq 98.0\%$, Shanghai lingfeng), glycolic acid ($\text{C}_2\text{H}_4\text{O}_3$, $\geq 98.0\%$, Sinopharm), ethylene glycol ($\text{C}_2\text{H}_6\text{O}_2$, $\geq 99.0\%$, Shanghai lingfeng), 2,3-dihydroxypropanoic acid ($\text{C}_3\text{H}_6\text{O}_4$, 20% in water, $\geq 95\%$, Macklin), potassium iodide (KI, $\geq 99.0\%$, Aladdin), bismuth(III) nitrate pentahydrate ($\text{Bi}(\text{NO}_3)_3 \cdot 5\text{H}_2\text{O}$, $\geq 99\%$, Macklin), potassium bicarbonate (KHCO_3 , $\geq 99.5\%$, Sinopharm), 2-isopropanol ($\text{C}_3\text{H}_8\text{O}$, $\geq 99.7\%$, Sinopharm), ethanol ($\text{C}_2\text{H}_6\text{O}$, $\geq 99.8\%$, Sinopharm), acetone ($\text{C}_3\text{H}_6\text{O}$, $\geq 99.5\%$), Nafion solution (5 wt%, D-chem), and carbon black (cabot vulcan xc-72c, Macklin) were used without further purification. Ni foam ($1.0 \text{ mm} \times 200 \text{ mm} \times 250 \text{ mm}$, surface density: 350 g/m^3 , aperture: 0.1 mm , porosity: 97.2% , Changde Liyuan New Materials Co., Ltd.) and Toray TGP-H-060 carbon paper ($2000 \text{ mm} \times 2000 \text{ mm} \times 0.19 \text{ mm}$) with fiber morphology were used as supporting materials of the catalytic electrode.

Synthesis of BiOI. Synthesis of BiOI microflower was adopted from the method reported by Hua Gui Yang et al,¹ but some adjustments were made appropriately. Specifically, 0.1245 g KI was dissolved in 10 mL ethylene glycol, and then 0.3613 g $\text{Bi}(\text{NO}_3)_3 \cdot 5\text{H}_2\text{O}$ was slowly added into the above solution under continuously stirring for 30 min to form a homogenous solution. The obtained solution was transferred to a 20 ml Teflon-lined stainless-steel autoclave, and then sealed and heated at $160 \text{ }^\circ\text{C}$ for 12 h . After the hydrothermal reaction, the sample was centrifuged and completely washed with DI water for 3 times. Finally, the sample collected by centrifugation was dried in a vacuum oven at $60 \text{ }^\circ\text{C}$ for 12 h .

Preparation of BiOI/CP electrode. Carbon paper (with $1 \times 1.25 \text{ cm}^2$ in total, and catalytic exposure areas of $1 \times 1 \text{ cm}^2$) was stepwise cleaned in acetone and water by

sonication for 30 min. The mixture of BiOI powder (10 mg) and carbon black (10 mg) were suspended in 2-propanol solution (920 μL) containing Nafion solution (80 μL) by sonicating dispersion. After sonication for 30 min, the slurry (200 μL) was dropped onto the carbon paper and formed a $1 \times 1 \text{ cm}^2$ uniform coating, which was then dried at room temperature for 12 h. The final loading quantity of the catalysts was *ca.* 2.0 mg cm^{-2} determined by electronic balance.

2. Definitions

Selectivity of formate formation from glycerol were determined by the following equation,

$$\text{Selectivity}(\%) = \frac{n_{\text{formate}} \times 1/3}{n_{0,\text{glycerol}} - n_{\text{glycerol}}} \times 100\% \quad (\text{S1})$$

where, n_{formate} is the molar amount of formate produced, $n_{0,\text{glycerol}}$ and n_{glycerol} are the initial and final molar amounts of glycerol before and after reaction, respectively.

Glycerol conversion (η_{glycerol} , %) was calculated using the following equation.

$$\eta_{\text{glycerol}}(\%) = \frac{n_{0,\text{glycerol}} - n_{\text{glycerol}}}{n_{0,\text{glycerol}}} \times 100\% \quad (\text{S2})$$

Faradaic efficiencies of formate from CO_2ER and GOR were calculated using the following equations, respectively.

$$\text{FE}_{\text{CO}_2\text{ER}}(\%) = \frac{n_{\text{c,formate}} \times 2 \times F}{Q} \times 100\% \quad (\text{S3})$$

$$\text{FE}_{\text{GOR}}(\%) = \frac{n_{\text{a,formate}} \times 8/3 \times F}{Q} \times 100\% \quad (\text{S4})$$

where $n_{\text{c,formate}}$ and $n_{\text{a,formate}}$ are the formate produced from the cathodic and anodic reactions, respectively, F is the Faraday constant ($96485.33 \text{ C mol}^{-1}$) and Q is the passed

charge (C).

All LSV curves in this work were not iR -corrected unless specified. If there was an iR -correction, the correction equation is as follow.

$$E_{corrected} = E_{measured} - iR_s \quad (S5)$$

where, $E_{corrected}$ is the potential after iR -correction, $E_{measured}$ is the measured potential, i is the measured current, R_s is the measured solution resistance.

3. Thermochemical calculation of the GOR-assisted CO₂ER

Standard Gibb's free energy and redox potential of reaction for the CO₂ER to formic acid (HCOOH) coupled with the GOR were calculated based on the following data. Standard molar Gibb's free energy of formation (ΔG_f):

C₃H₈O₃ (l): -478.6 kJ mol⁻¹,

OH⁻ (l): -157.244 kJ mol⁻¹,

HCOOH (l): -361.3 kJ mol⁻¹,

H₂O (l): -237.13 kJ mol⁻¹,

CO₂(g): -394.38 kJ mol⁻¹.

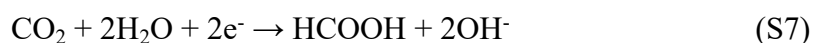
For anode reaction (GOR):



$\Delta G_{anode} = -532.998$ KJ mol⁻¹

$\varphi_{Anode} = -0.69$ V vs. SHE

For cathode reaction (CO₂ER):



$\Delta G_{Cathode} = 192.852$ KJ mol⁻¹

$\varphi_{Cathode} = -1.0$ V vs. SHE

For overall reaction :



$$\Delta G_{\text{Overall}} = 238.41 \text{ KJ mol}^{-1}$$

$$E_{\text{Overall}} = 0.31 \text{ V}$$

Note: $\varphi_{\text{Anode}} = \Delta G_{\text{Anode}} / (z \times F)$, $\varphi_{\text{Cathode}} = -\Delta G_{\text{Cathode}} / (z \times F)$, where z is the number of electrons transferred and F is the Faraday constant (96485.33 C mol⁻¹).

$E_{\text{Overall}} = \varphi_{\text{Anode}} - \varphi_{\text{Cathode}}$. All thermodynamic properties are reported under standard conditions (1 bar and 298 K).

4. Calculation of the energy saving

The direct energy consumption of producing a certain amount of formate from CO₂ER and GOR could be calculated by the formula: $W = U \times I \times t = U \times Q$, where U is the applied cell voltage (V), I is the current (A), t is the time (s), and Q is the passed charge (C). Assuming the electrical energy consumption of GOR-CO₂ER system was $W_1 = U_1 \times Q_1$, while the OER-CO₂ER system was $W_2 = U_2 \times Q_2$, when producing the same amount of formate, the required electron is identical. This means $Q_1 = Q_2$. Therefore, the energy saving of GOR-CO₂ER compared to OER-CO₂ER was $(W_2 - W_1) / W_2 = (U_2 - U_1) / U_2$. Based on this, the energy consumption saving was calculated as follow :

(1) the voltage of GOR-CO₂ER system was 1.658 V at 5 mA cm⁻², while that of the OER-CO₂ER system was 1.825 V. The energy consumption saving at 5 mA cm⁻² was $(1.825 - 1.658) / 1.825 \times 100\% = 9.2\%$.

(2) the voltage of GOR-CO₂ER system was 1.742 V at 10 mA cm⁻², while that of the OER-CO₂ER system was 1.974 V. The energy consumption saving at 10 mA cm⁻² was $(1.974 - 1.742) / 1.974 \times 100\% = 11.8\%$.

(3) the voltage of GOR-CO₂ER system was 1.809 V at 15 mA cm⁻², while that of the OER-CO₂ER system was 2.087 V. The energy consumption saving at 15 mA cm⁻² was $(2.087-1.809)/2.087 \times 100\% = 13.3\%$.

(4) the voltage of GOR-CO₂ER system was 1.872 V at 20 mA cm⁻², while the OER-CO₂ER system was 2.175 V. The energy consumption saving at 20 mA cm⁻² was $(2.175-1.872)/2.175 \times 100\% = 13.9\%$.

5. Electricity-to-formate energy conversion efficiency

The electricity-to-formate energy conversion efficiency of the GOR-CO₂ER was calculated as follows:

$$\eta = \frac{n_{\text{formate}} \times \Delta H^{\circ}}{Q \times U} \quad (\text{S9})$$

where ΔH° (= 254 kJ mol⁻¹) is the heating value of formate, which is calculated from Eq. S10, where n_{formate} is the summarized molar amount of formate produced from both the cathode and anode sides, U is the cell voltage (V), Q is the passed charge (C).

$$\Delta H^{\circ}(298.15 \text{ K}) = \left| \Delta_f H^{\circ}(\text{CO}_2) + \Delta_f H^{\circ}(\text{H}_2\text{O}) - \Delta_f H^{\circ}(\text{HCOO}^-) - \frac{1}{2} \Delta_f H^{\circ}(\text{O}_2) \right| \quad (\text{S10})$$

At the optimal point, the amount of formate produced by GOR (anode) and CO₂ER (cathode) was 0.107 mmol and 0.146 mmol, respectively. The applied voltage and amount of passed charge was 1.9 V and 30.78 C, respectively. The energy of formate obtained by the GOR-CO₂ER system was $n_{\text{formate}} \times \Delta H^{\circ} = (0.107 + 0.146) \times 254 = 64.26 \text{ J}$, while the electricity consumption was $Q \times U = 30.78 \times 1.9 = 58.48 \text{ J}$. Therefore, the electricity-to-formate energy conversion efficiency of the GOR-CO₂ER system was $\eta = 64.26/58.48 \times 100\% = 109.9\%$.

Results obtained for characterizations, experiments and calculations



Fig. S1 Schematic illustration of the $\text{Ni}_x\text{Co}_{1-x}(\text{OH})_2@\text{HOS}/\text{NF}$ preparation.

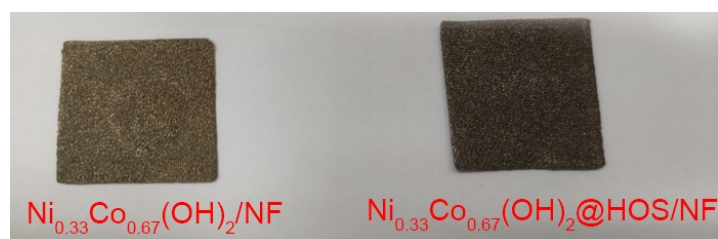


Fig. S2 Optical photographs of the $\text{Ni}_{0.33}\text{Co}_{0.67}(\text{OH})_2/\text{NF}$ and $\text{Ni}_{0.33}\text{Co}_{0.67}(\text{OH})_2@\text{HOS}/\text{NF}$.

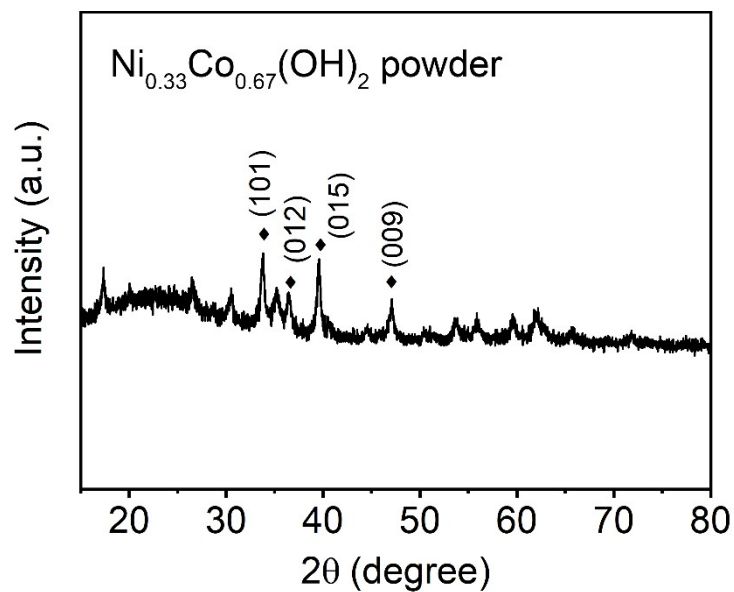


Fig. S3 XRD pattern of $\text{Ni}_{0.33}\text{Co}_{0.67}(\text{OH})_2$ powder.

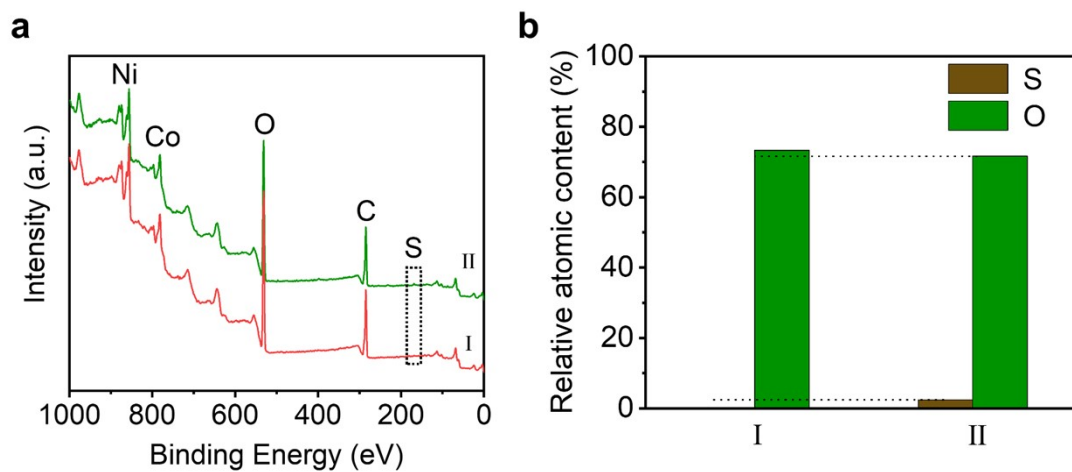


Fig. S4 (a) Full XPS spectra of $\text{Ni}_{0.33}\text{Co}_{0.67}(\text{OH})_2/\text{NF}$ (I) and $\text{Ni}_{0.33}\text{Co}_{0.67}(\text{OH})_2@\text{HOS}/\text{NF}$ (II); (b) relative atomic contents of S and O in $\text{Ni}_{0.33}\text{Co}_{0.67}(\text{OH})_2/\text{NF}$ (I) and $\text{Ni}_{0.33}\text{Co}_{0.67}(\text{OH})_2@\text{HOS}/\text{NF}$ (II).

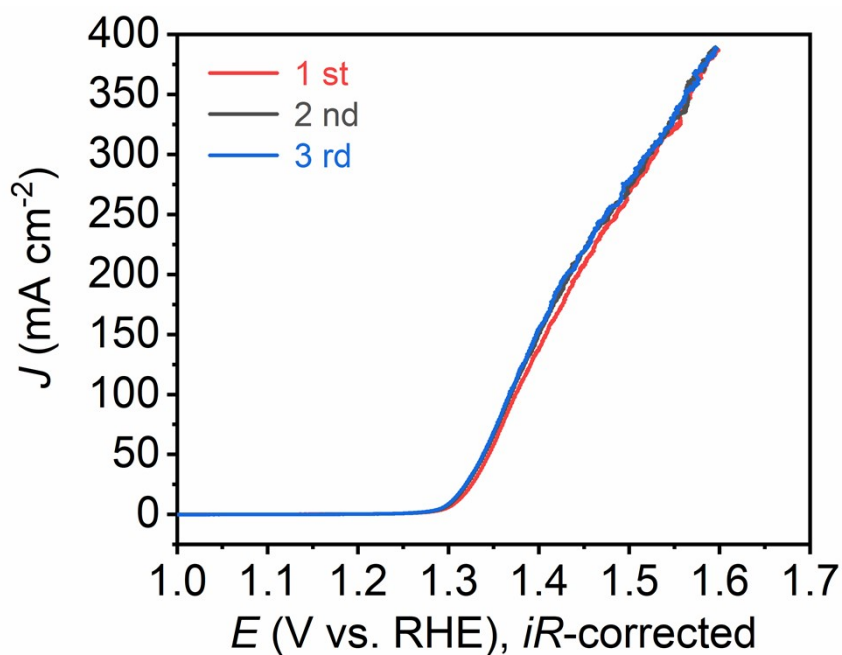


Fig. S5 Three successive LSV curves of $\text{Ni}_{0.33}\text{Co}_{0.67}(\text{OH})_2@\text{HOS}/\text{NF}$ anode in 1 mol L^{-1} KOH with 0.1 mol L^{-1} glycerol (scan rate: 10 mV s^{-1}).

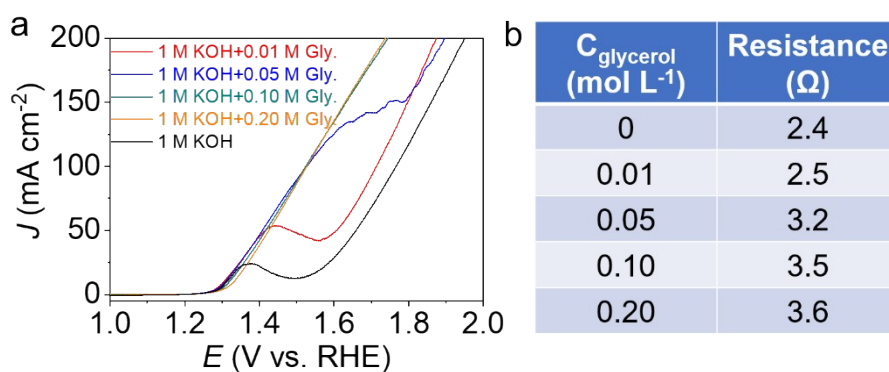


Fig. S6 (a) Glycerol anodic oxidation polarization curves on $\text{Ni}_{0.33}\text{Co}_{0.67}(\text{OH})_2@\text{HOS}/\text{NF}$ electrode in 1 mol L^{-1} KOH with varied glycerol concentrations (Gly: glycerol; scan rate: 10 mV s^{-1}); (b) the corresponding resistance between the working and reference electrodes.

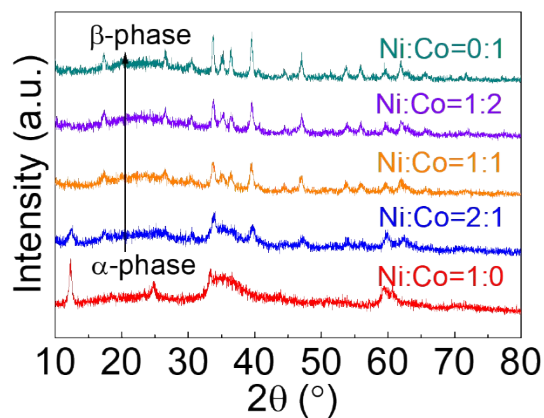


Fig. S7 XRD patterns of $\text{Ni}_x\text{Co}_{1-x}(\text{OH})_2$ powders. XRD patterns showed that the crystal phase of metal hydroxides gradually transferred from the alkaline-unstable α -phase to the alkaline-stable β -phase with Co-content increase.

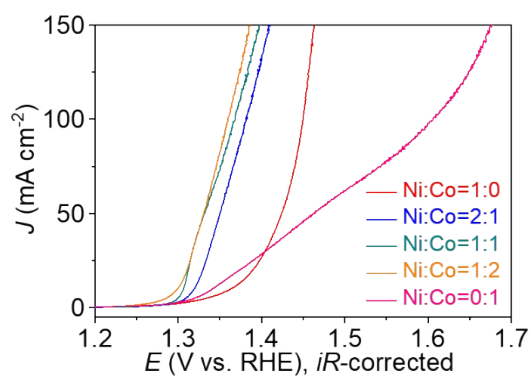


Fig. S8 Comparison of the electrocatalytic performance of the $\text{Ni}_x\text{Co}_{1-x}(\text{OH})_2@HOS/NF$ electrodes with different Ni:Co molar ratios in 1 mol L^{-1} KOH + 0.1 mol L^{-1} glycerol with a scan rate of 10 mV s^{-1} .

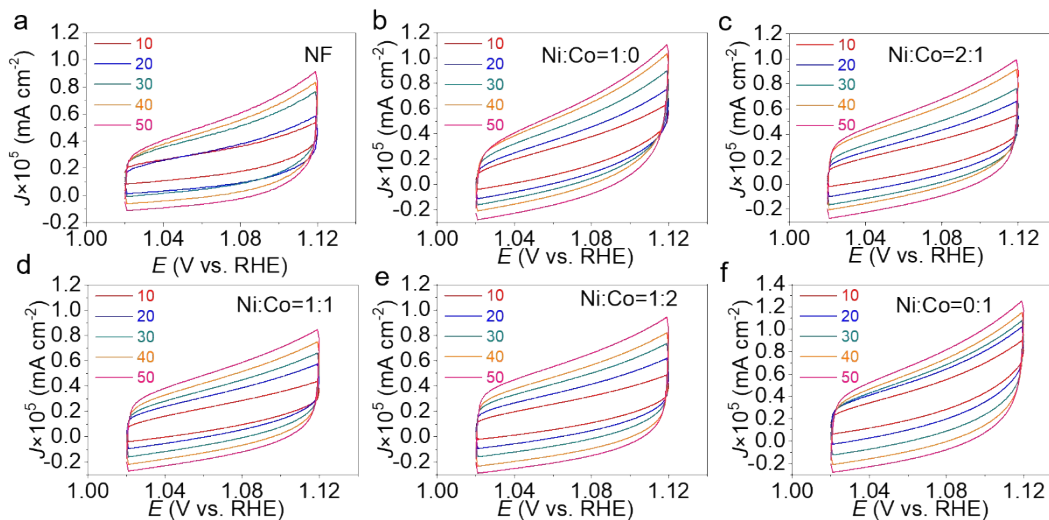


Fig. S9 CV curves for ECSA analysis of the NF and $\text{Ni}_x\text{Co}_{1-x}(\text{OH})_2@HOS/NF$ electrodes with different Ni:Co molar ratios in 1 mol L^{-1} KOH with 0.1 mol L^{-1} glycerol at different scan rates from 10 to 50 mV s^{-1} .

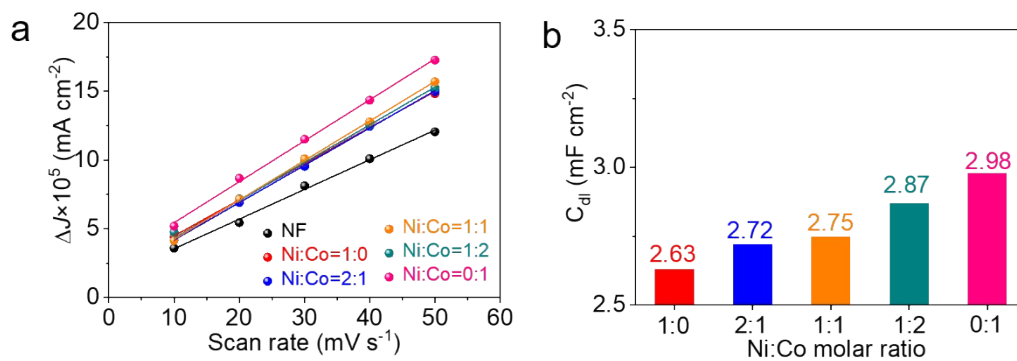


Fig. S10 C_{dl} (a) fitting curves and (b) values of the NF and $\text{Ni}_x\text{Co}_{1-x}(\text{OH})_2@HOS/NF$ electrodes.

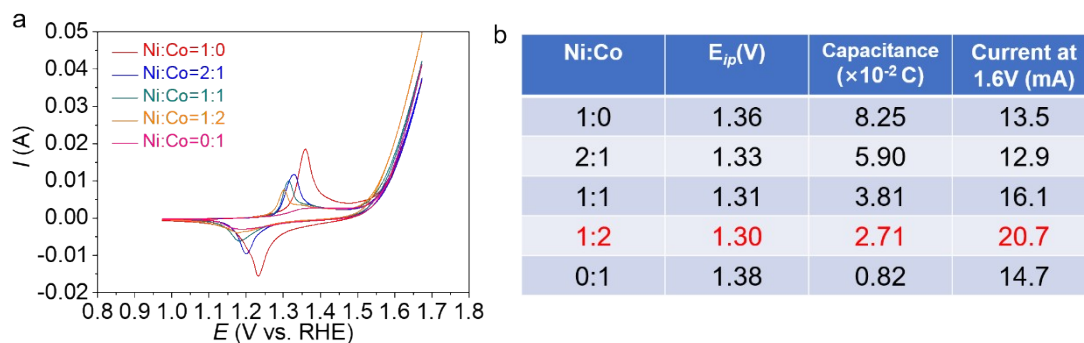


Fig. S11 (a) CV curves of the $\text{Ni}_x\text{Co}_{1-x}(\text{OH})_2@\text{HOS}/\text{NF}$ electrodes with different Ni:Co molar ratios in the 1 mol L^{-1} KOH electrolyte with a scan rate of 5 mV s^{-1} ; (b) Table of the corresponding anodic E_{ip} , capacitances, and the OER currents at 1.6 V vs. RHE.

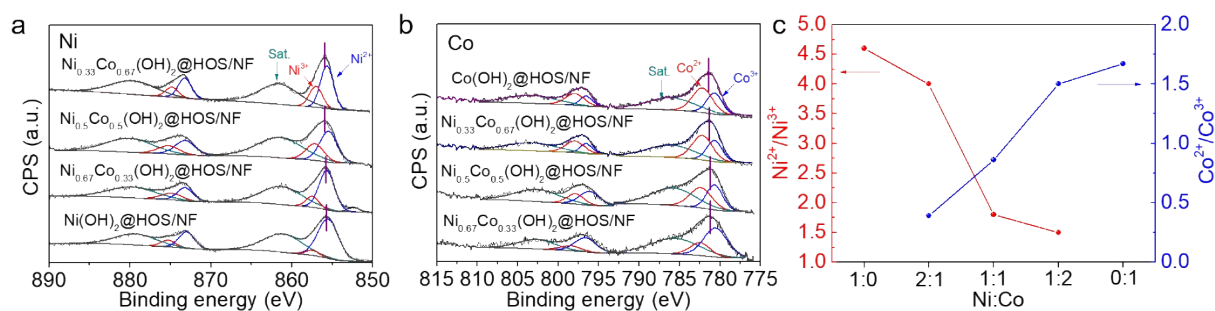


Fig. S12 XPS analysis of the $\text{Ni}_x\text{Co}_{1-x}(\text{OH})_2@\text{HOS}/\text{NF}$ electrodes: (a) Ni 2p, (b) Co 2p, and (c) ratios of $\text{M}^{2+}/\text{M}^{3+}$ (M represents Co and Ni).

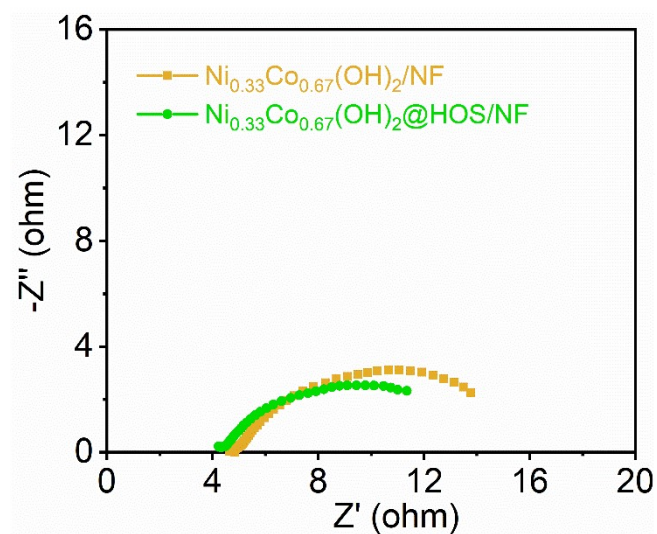


Fig. S13 Electrochemical impedance spectroscopy (EIS) of $\text{Ni}_{0.33}\text{Co}_{0.67}(\text{OH})_2/\text{NF}$ and $\text{Ni}_{0.33}\text{Co}_{0.67}(\text{OH})_2@\text{HOS}/\text{NF}$ in 1 mol L^{-1} KOH with 0.1 mol L^{-1} glycerol.

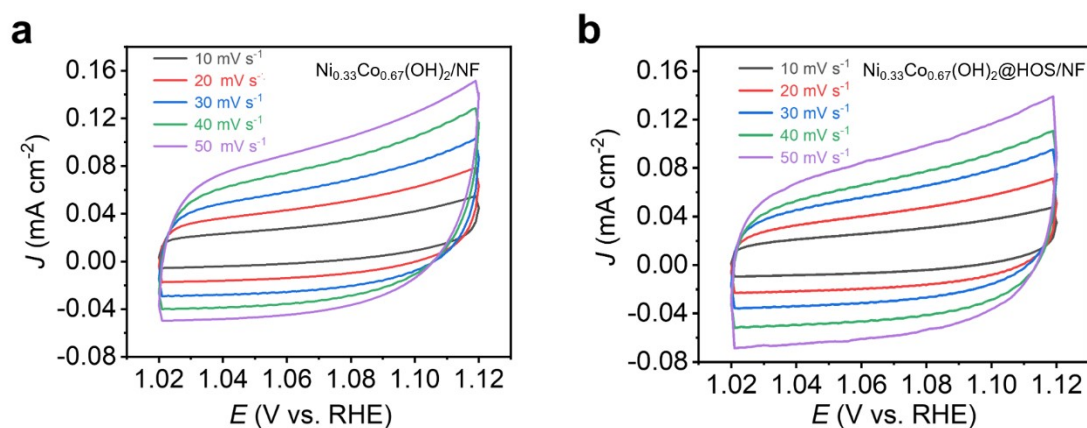


Fig. S14 Electrochemical surface area (ECSA) test in 1 mol L^{-1} KOH with 0.1 mol L^{-1} glycerol at different scan rates from 10 to 50 mV s^{-1} for (a) $\text{Ni}_{0.33}\text{Co}_{0.67}(\text{OH})_2/\text{NF}$ and (b) $\text{Ni}_{0.33}\text{Co}_{0.67}(\text{OH})_2@\text{HOS}/\text{NF}$.

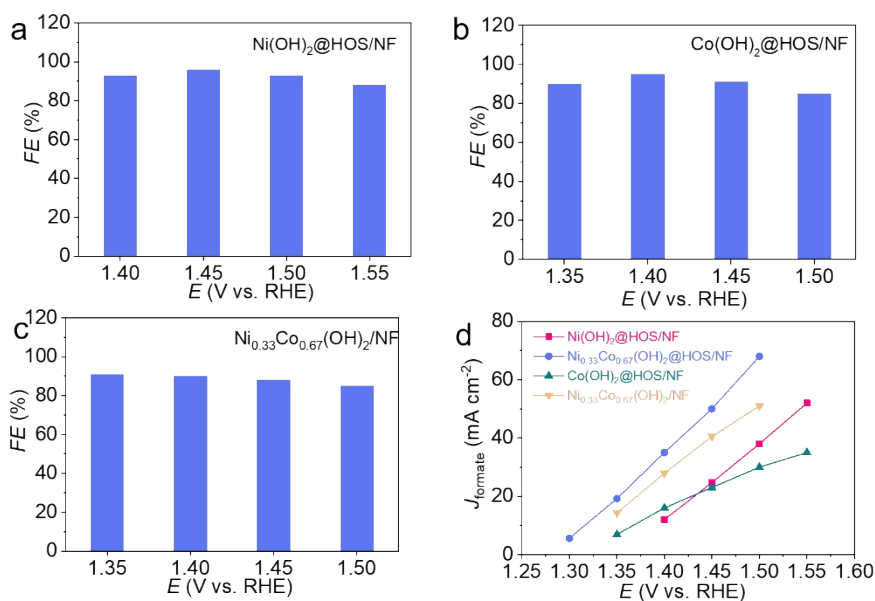


Fig S15 FEs of formate production from GOR on the (a) $\text{Ni}(\text{OH})_2@/\text{HOS}/\text{NF}$, (b) $\text{Co}(\text{OH})_2@/\text{HOS}/\text{NF}$, and (c) $\text{Ni}_{0.33}\text{Co}_{0.67}(\text{OH})_2/\text{NF}$ electrodes in 1 mol L^{-1} KOH solution containing 0.1 mol L^{-1} glycerol (reaction time: 30 min); (d) corresponding partial current densities of the formate production.

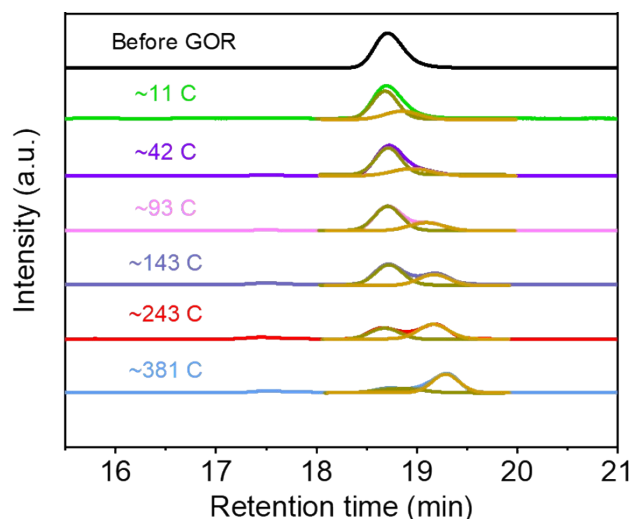


Fig. S16 HPLC chromatograms of the reaction products from the electrochemical oxidation of glycerol on $\text{Ni}_{0.33}\text{Co}_{0.67}(\text{OH})_2@/\text{HOS}/\text{NF}$ electrode at a constant potential of 1.35 V vs. RHE in 1 mol L^{-1} KOH solution containing 0.1 mol L^{-1} glycerol with different amounts of total charge transferred.

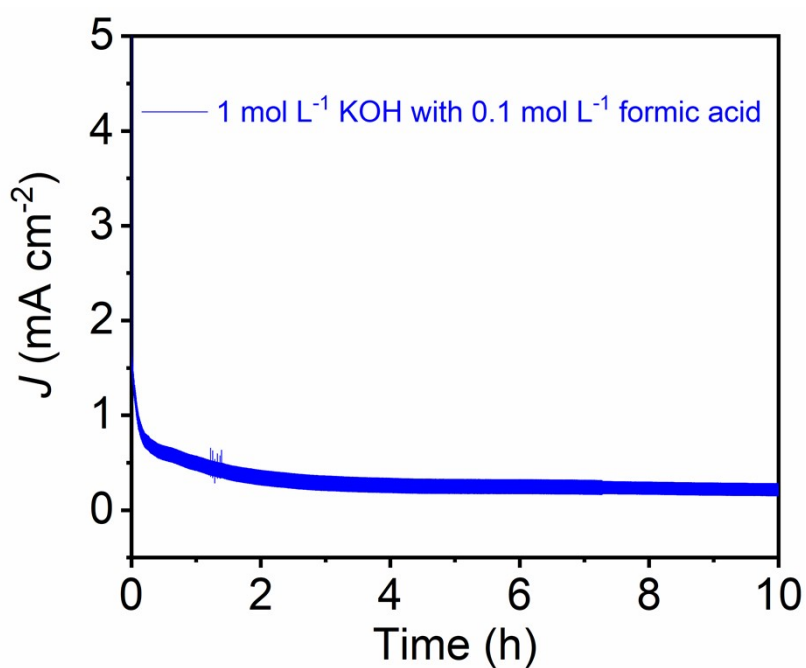


Fig. S17 J-t curve obtained on $\text{Ni}_{0.33}\text{Co}_{0.67}(\text{OH})_2@\text{HOS}/\text{NF}$ electrode at a constant potential of 1.35 V vs. RHE in 1 mol L⁻¹ KOH solution containing 0.1 mol L⁻¹ formic acid.

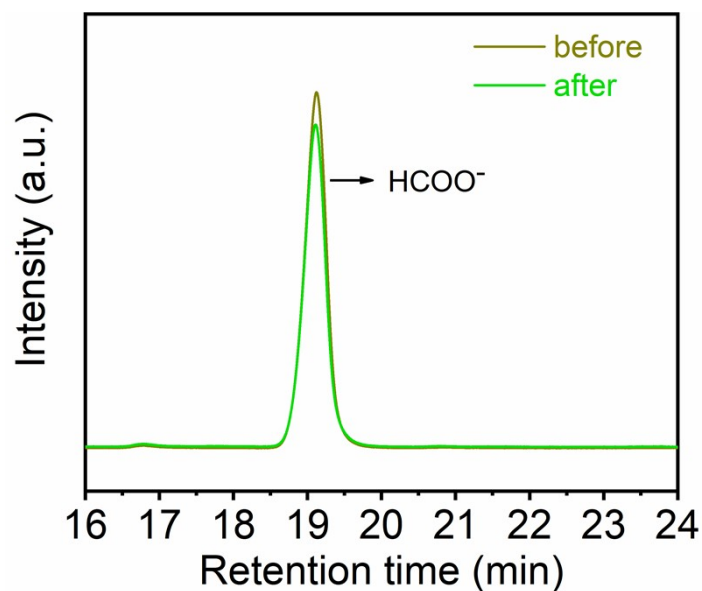


Fig. S18 HPLC chromatograms of the formate before and after 10 h anodic oxidation on $\text{Ni}_{0.33}\text{Co}_{0.67}(\text{OH})_2@\text{HOS}/\text{NF}$ electrode in 1.0 mol L⁻¹ KOH solution containing 0.1 mol L⁻¹ formic acid.

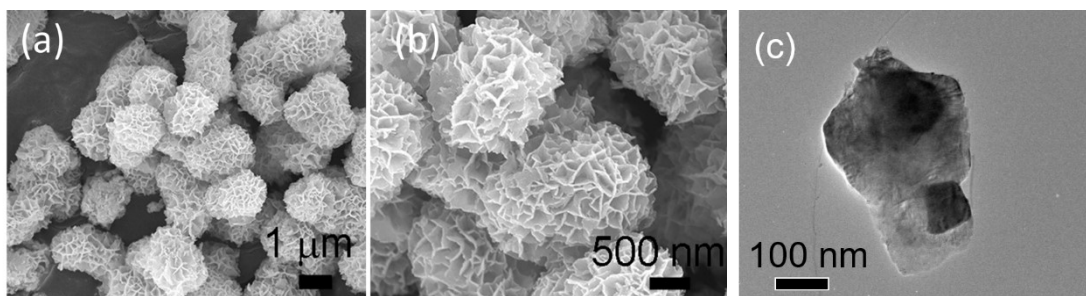


Fig. S19 SEM (a,b) and TEM (c) images of the pristine BiOI.

The as-prepared BiOI catalyst showed a microflower morphology, which was destroyed and converted to stacked nanosheets and particles after CO₂ER for about 1 h (at -1.0 V vs. RHE), indicating that the pristine BiOI microflower could undergo reduction to generate layered oxidized Bi₂O₂CO₃ and metallic Bi components. This is in accordance with previous report.¹

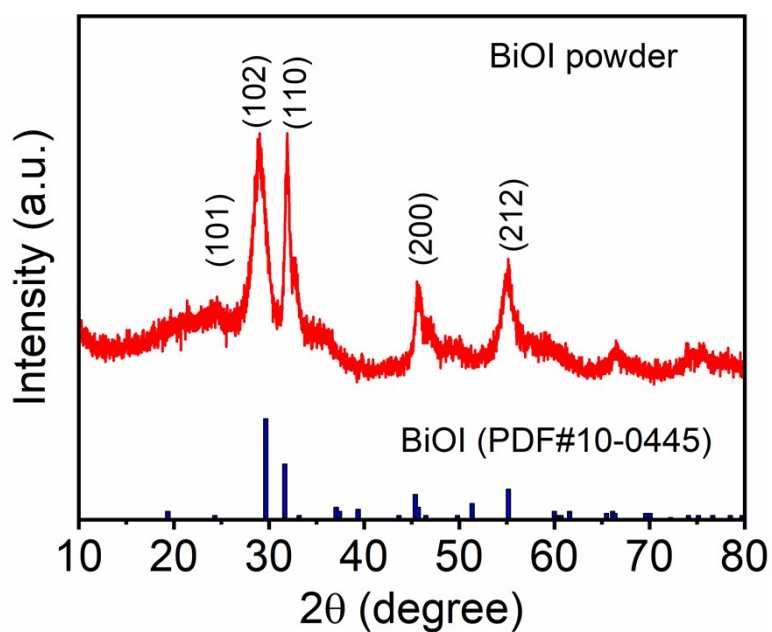


Fig. S20 XRD pattern of as-prepared BiOI microflowers.

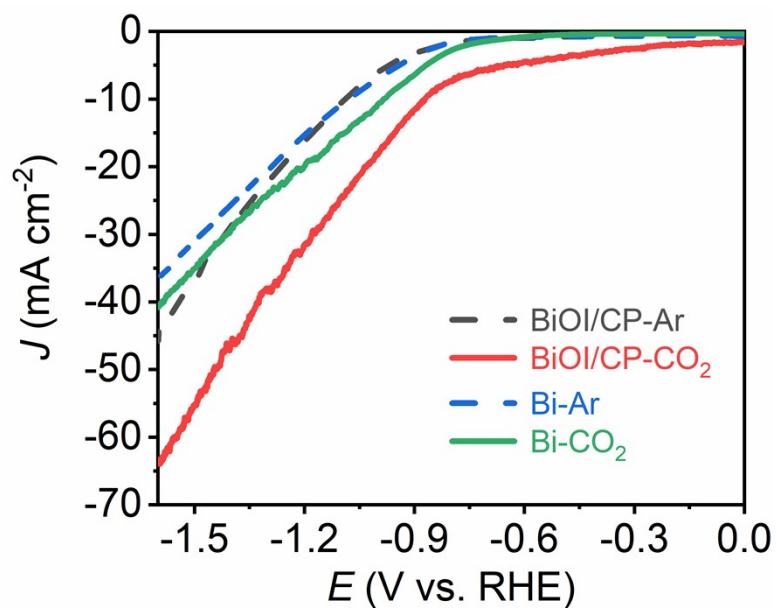


Fig. S21 LSV curves of BiOI/CP and controlled samples in CO₂-saturated or Ar-saturated 0.5 mol L⁻¹ KHCO₃ aqueous solution (scan rate:10 mV s⁻¹).

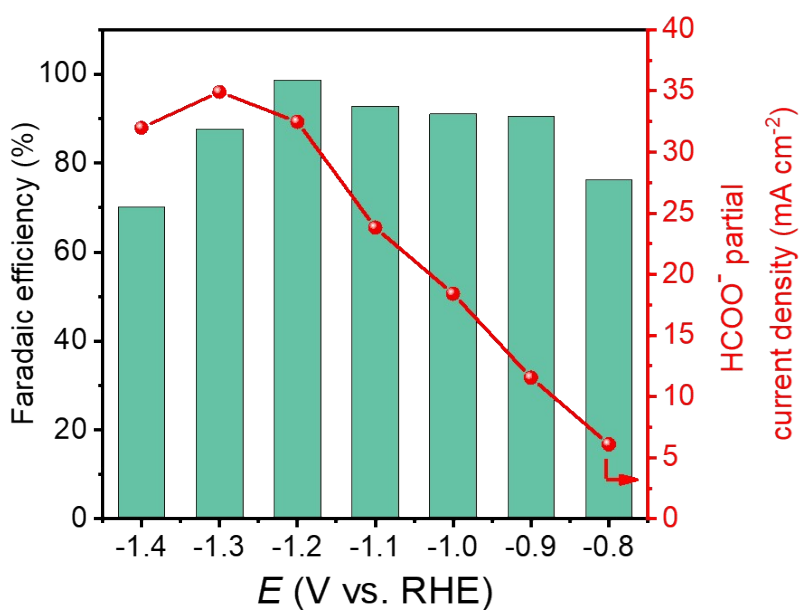


Fig. S22 Faradaic efficiencies and partial current density of HCOO⁻ from the electrochemical reduction of CO₂ in 0.5 mol L⁻¹ KHCO₃ electrolyte saturated with CO₂ at different potentials on BiOI/CP electrode.

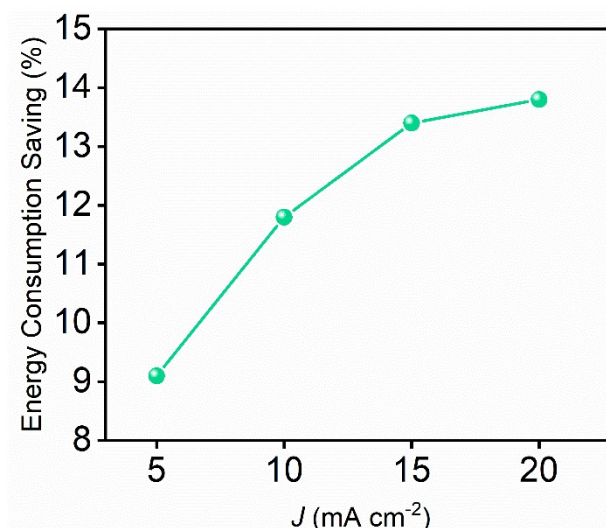


Fig. S23 Energy consumption savings of GOR-assisted CO₂ER compared to normal CO₂ER at different current densities (reaction conditions: cathode compartment contained CO₂-saturated 0.5 mol L⁻¹ KHCO₃ solution, anode compartment contained 1 mol L⁻¹ KOH with or without 0.1 mol L⁻¹ glycerol).

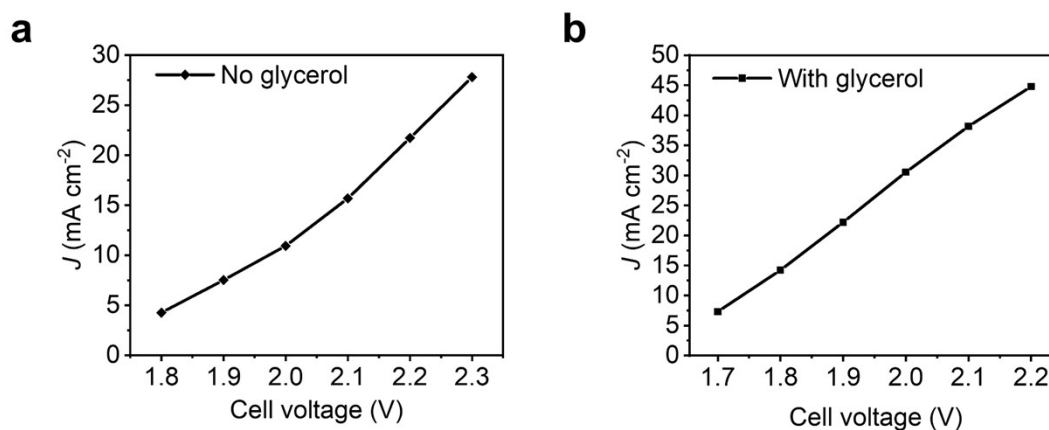


Fig. S24 Cell voltage-dependent current density of the two-electrode electrolysis with (a) and without (b) glycerol in the anodic chamber (reaction condition: cathode compartment contained CO₂-saturated 0.5 mol L⁻¹ KHCO₃ solution, anode compartment contained 1 mol L⁻¹ KOH with or without 0.1 mol L⁻¹ glycerol, cathode: BiOI/CP, anode: Ni_{0.33}Co_{0.67}(OH)₂@HOS/NF).

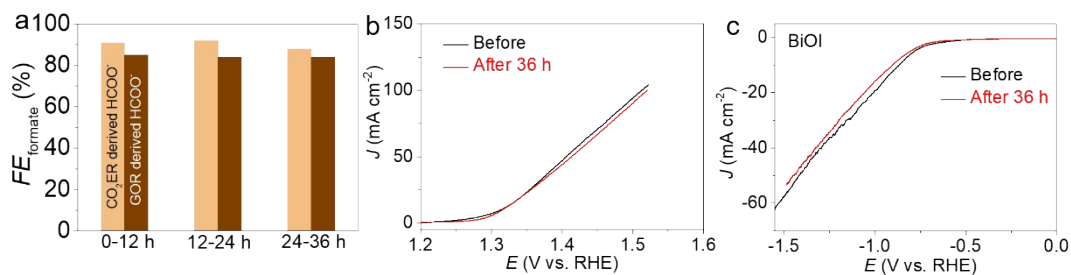


Fig. S25 (a) FEs of formate production from the CO₂ER+GOR system at 1.8 V for 36-h electrolysis; comparison of the electrochemical performance of (b) Ni_{0.33}Co_{0.67}(OH)₂@HOS/NF and (c) BiOI/CP electrodes before and after the 36-h electrolysis.

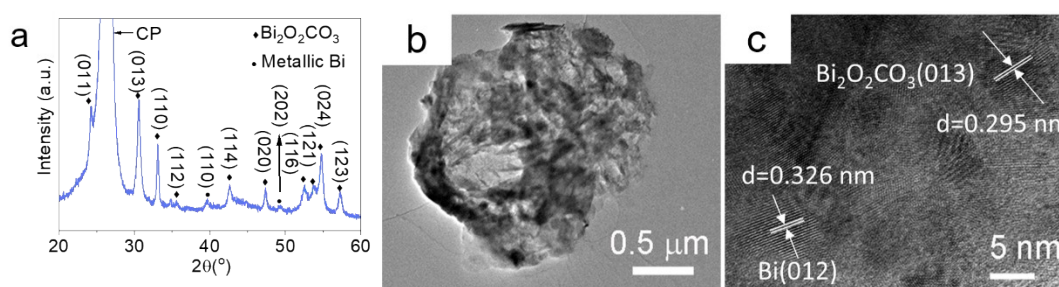


Fig. S26 (a) XRD pattern, (b) TEM, and (c) HRTEM images of the BiOI/CP electrode after the 36-h electrolysis.

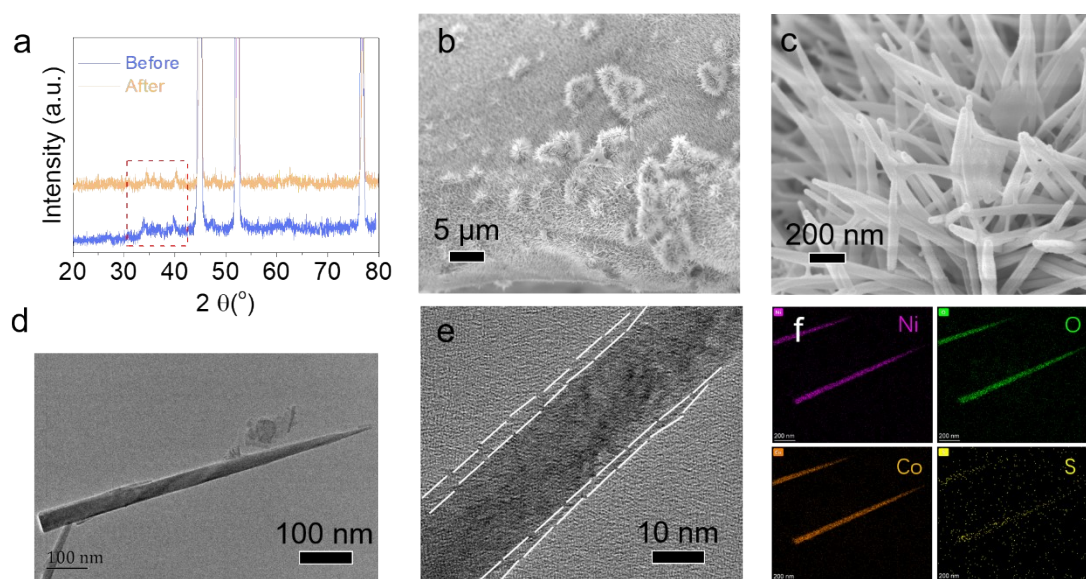


Fig. S27 Characterizations of the $\text{Ni}_{0.33}\text{Co}_{0.67}(\text{OH})_2@\text{HOS}/\text{NF}$ electrode after the 36-h electrolysis: (a) XRD patterns, (b,c) SEM, (d) TEM, and (e) EDS mapping images.

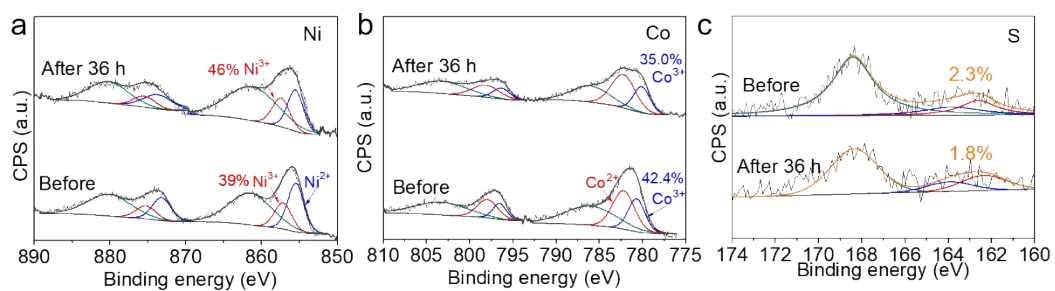


Fig. S28 XPS spectra of the $\text{Ni}_{0.33}\text{Co}_{0.67}(\text{OH})_2@\text{HOS}/\text{NF}$ electrode after the 36-h electrolysis: (a) Ni 2p, (b) Co 2p, and (c) S 2p.

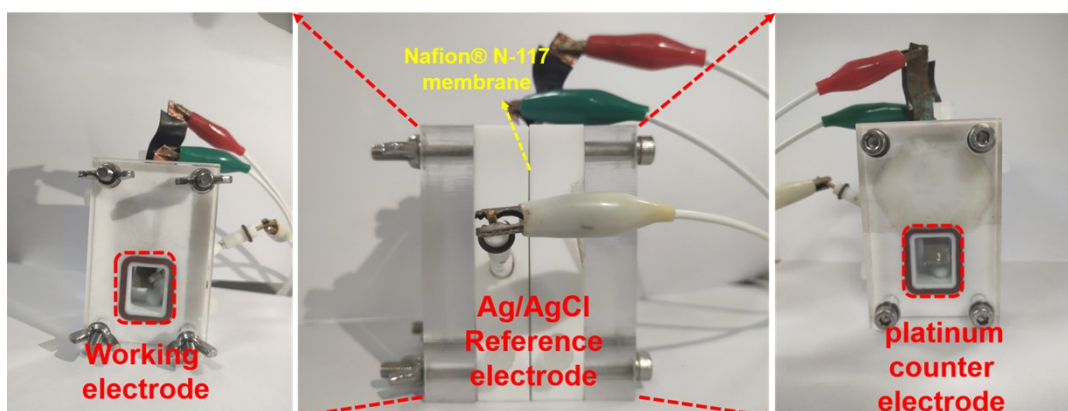


Fig. S29 Photographs of the two-chamber three-electrode cell.

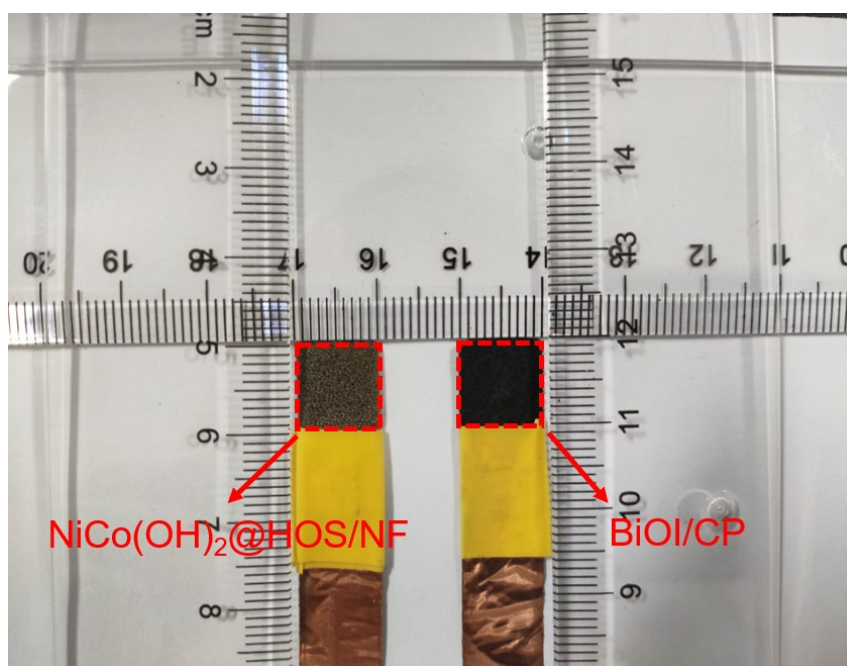


Fig. S30 Photograph of the Ni_{0.33}Co_{0.67}(OH)₂@HOS/NF electrode and BiOI/CP electrode (epoxy resins and yellow insulating tape are applied to define the geometric area of the electrodes (1 cm²)).

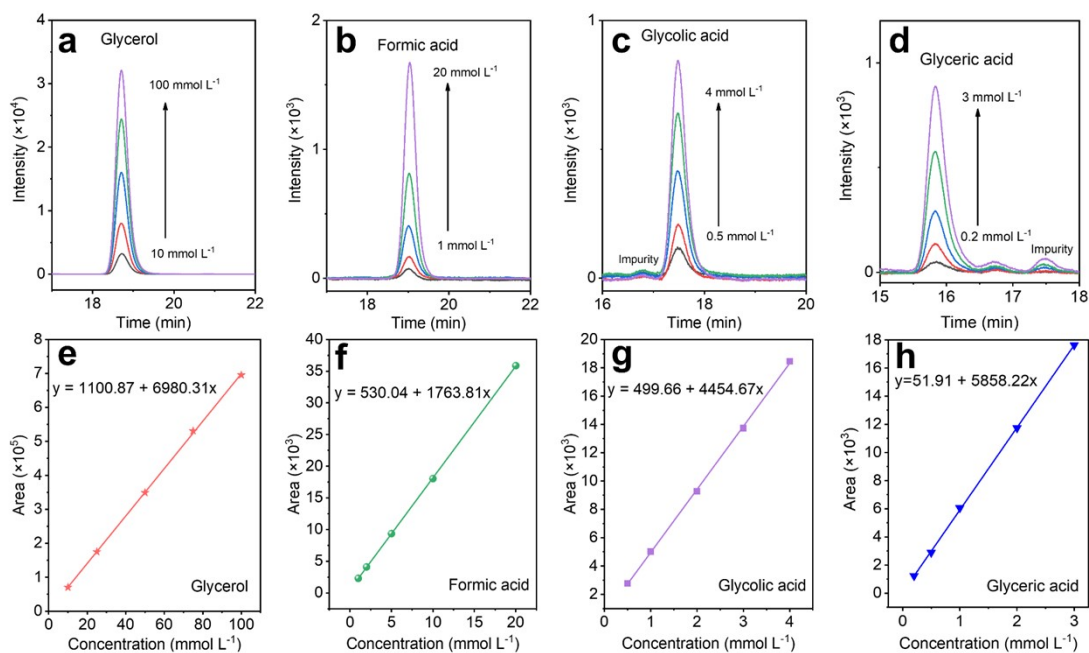


Fig. S31 Standard HPLC chromatograms of glycerol and its possible oxidation products in various concentrations (standard HPLC chromatograms of (a) glycerol, (b) formic acid, (c) glycolic acid, and (d) glyceric acid; (e-h) corresponding calibration curves used for quantification).

Table S1 Comparison of the reported transition-metal based electrocatalysts for the OOR-assisted hydrogen evolution reaction

Catalyst	Electrolyte	Anodic product	η_{OOR} (V vs RHE) ^a	Tafel slope (mV dec ⁻¹)	Reference
Ni-Mo-N/CFC	1 mol L ⁻¹ KOH + 0.1 mol L ⁻¹ glycerol	formate	1.30	87	[2]
Ni ₃ C NPs	1 mol L ⁻¹ KOH + 1.0 mol L ⁻¹ methanol	formate	1.43	-	[3]
MMCN	1 mol L ⁻¹ KOH + 0.5 mol L ⁻¹ urea	N ₂ , CO ₂	1.33	72	[4]
NiFe-LDH	1 mol L ⁻¹ KOH + 10 mmol L ⁻¹ HMF	FDCA	1.37	75	[5]
Ni ₂ P/Ni/NF	1 mol L ⁻¹ KOH + 30 mmol L ⁻¹ furfural	2-furoic acid	1.34	-	[6]
NiSe nanorod	1 mol L ⁻¹ KOH + 1 mmol L ⁻¹ benzylamine	benzonitrile	1.34	-	[7]
Ni_{0.33}Co_{0.67}(OH)₂@HOS/NF	1 mol L⁻¹ KOH + 0.1 mol L⁻¹ glycerol	formate	1.30	35	This work

^a η_{OOR} : potential for organic oxidation reaction, recorded at a current density of 10 mA cm⁻².

References

- 1 P. F. Liu, M. Y. Zu, L. R. Zheng and H. G. Yang, *Chem. Commun.*, 2019, **55**, 12392-12395.
- 2 Y. Li, X. Wei, L. Chen, J. Shi and M. He, *Nat. Commun.*, 2019, **10**, 5335.
- 3 J. Li, R. Wei, X. Wang, Y. Zuo, X. Han, J. Arbiol, J. Llorca, Y. Yang, A. Cabot and C. Cui, *Angew. Chem. Int. Ed.*, 2020, **59**, 20826-20830.
- 4 C. Xiao, S. Li, X. Zhang and D. R. MacFarlane, *J. Mater. Chem. A*, 2017, **5**, 7825-7832.
- 5 W.-J. Liu, L. Dang, Z. Xu, H.-Q. Yu, S. Jin and G. W. Huber, *ACS Catal.*, 2018, **8**, 5533-5541.
- 6 N. Jiang, X. Liu, J. M. Dong, B. You, X. Liu and Y. Sun, *ChemNanoMat*, 2017, **3**, 491-495.
- 7 Y. Huang, X. D. Chong, C. B. Liu, Y. Liang and B. Zhang, *Angew. Chem. Int. Ed.*, 2018, **57**, 13163-13166.